

RESEARCH

Open Access



# Influence of Nano-silica on the Leaching Attack upon Photocatalytic Cement Mortars

Atta-ur-Rehman, Abdul Qudoos, Sadam Hussain Jakhriani, Hong Gi Kim and Jae-Suk Ryou\*

## Abstract

Photocatalytic cementitious materials are used in the exterior of the buildings and infrastructure for self-cleaning and air-purifying purposes. These materials are exposed to the aggressive exposure conditions like acid rain, runoff water and are subjected to the deterioration due to the leaching of calcium. The knowledge of leaching attack upon photocatalytic cementitious materials after the addition of nano-materials is necessary. In the current study, the influence of nano-silica addition on the leaching attack upon photocatalytic cement mortars was thoroughly investigated. For this purpose, photocatalytic mortars were made by adding 3% TiO<sub>2</sub> and variable amount (0–2%) of nano-silica. Accelerated leaching environment was created by immersing mortars in 6 M ammonium nitrate (NH<sub>4</sub>NO<sub>3</sub>) solution. The progressive development of the leaching depth in mortars was measured. The loss of hardened properties was monitored by evaluating the compressive strength, flexural strength, porosity, and dynamic modulus of elasticity. X-ray diffraction, thermogravimetry, Fourier transform infrared spectroscopy, scanning electron microscopy tests were conducted to know the microstructural deteriorations. Results indicated that the leaching attack induced mechanical and microstructural damages in the mortars, but the addition of nano-silica decreased mechanical and microstructural damages in the photocatalytic mortars and increased the resistance of photocatalytic mortars to leaching attack.

**Keywords:** nano-titanium dioxide, nano-silica, photocatalytic mortars, decalcification, durability, leaching, deterioration

## 1 Introduction

Titanium dioxide (TiO<sub>2</sub>) is added in concrete to make self-cleaning, anti-bacterial, and air-purifying concrete (Li et al. 2018; Staub de Melo et al. 2018; Binas et al. 2018; Guo and Poon 2018; Seo and Yun 2017; Han et al. 2017). Such a concrete is used in the various parts of structures which are exposed to the sun light as TiO<sub>2</sub> needs sunlight to perform its beneficial roles (Diamanti et al. 2015; Banerjee et al. 2015). Examples of TiO<sub>2</sub> containing concrete structures can be building exterior, pavement blocks, road kerbs (Paolini et al. 2018; Pozo-Antonio and Dionísio 2017; García et al. 2018). Photocatalytic concrete should be resistant to the aggressive environments for long term services, but it is a porous material (Mohseni et al. 2016). Due to its exposure to the

atmosphere, it can be attacked by the external chemical agents during its service life which reduce its strength and serviceability (Han et al. 2014; Atta-ur-Rehman et al. 2018). Additionally, photocatalytic process occurs at the surface of concrete (Tobaldi et al. 2017). The modification of the surface of concrete by chemical and physical agents can affect the photocatalysis, so photocatalytic mortars should be made durable (Hassan et al. 2010). Examples of external aggressive chemical agents which can attack photocatalytic concrete are acid rain, carbon dioxide and water showers (Berger et al. 2013; Park et al. 2018; Yang et al. 2018). When they penetrate in the pores of the concrete, a concentration gradient of Ca<sup>+</sup> ions is generated (Kamali et al. 2008). Consequently, hydrated products; portlandite (CH), calcium-silicate-hydrate (CSH), AFm, AFt, Friedel's salt, are dissolved and ions are diffused in the pore water. The order of their solubility is CH > AFm > Friedel's salt > AFt > CSH (Puertas et al. 2012). The solubility of these products occurs slowly but it alters the microstructure and leaves behind the pores

\*Correspondence: jsryou@hanyang.ac.kr  
Department of Civil and Environmental Engineering, Hanyang University,  
222, Wangsimni-ro, Seongdong-gu, Seoul 04763, South Korea  
Journal information: ISSN 1976-0485 / eISSN 2234-1315

and increases the porosity (Phung et al. 2016; Lafhaj and Goueygou 2009; Xiong et al. 2016). As hydration products contribute to the strength of the mortars, their decalcification can reduce the strength of the photocatalytic mortars.

Use of nano-silica is getting attention of researchers and constructors (Singh et al. 2013). It is a pozzolanic material and can be added in the concrete as an alternative to silica fume (Khaloo et al. 2016). It reacts with portlandite and produces additional calcium-silicate-hydrate gels (Zhang et al. 2016). Nano-silica changes the fresh, hardened, and microstructure properties of photocatalytic mortars (Sikora et al. 2017; Mendoza et al. 2015; Senff et al. 2012; Eom et al. 2019). It effects the durability properties like carbonation and chloride penetration (Mohseni et al. 2015). Addition of nano-silica increases the strength in photocatalytic cement-based materials and it does not reduce the photocatalytic performance (Wang et al. 2018; Mendoza et al. 2015). It can have effects on the leaching attack upon photocatalytic mortars, but it has not been yet explored. This study focuses on the decalcification of hydration products after the addition of nano-silica in photocatalytic cement mortars. Five mortar types were made by adding 0%, 0.5%, 1%, 1.5%, and 2% nano-silica in photocatalytic mortars. In order to accelerate the leaching attack, 6 M solution of  $\text{NH}_4\text{NO}_3$  solution was used as aggressive medium (Tang et al. 2016). This concentrated  $\text{NH}_4\text{NO}_3$  solution can accelerate the dissolution by 300 times compared to the deionized water (Segura et al. 2013). After immersion in  $\text{NH}_4\text{NO}_3$  solution, the evolution of leaching depth was thoroughly monitored in mortars. The compressive, flexural strengths, dynamic modulus of elasticity, mercury intrusion porosimetry (MIP), water porosity were measured, and a comparison was conducted with controlled mortars. Three replicates were tested for each mortar type and mean values are reported in this paper. X-ray diffraction (XRD), thermogravimetry (TGA), Fourier transform infrared spectroscopy (FTIR), scanning electron microscopy (SEM) analysis were conducted to evaluate the microstructural damages.

## 2 Materials and Experimental Programs

### 2.1 Materials

The photocatalytic mortars were composed of fine aggregate, ordinary Portland cement, water and  $\text{TiO}_2$ . The fineness modulus and specific gravity of fine aggregate were 2.74 and 2.6, respectively. The fine aggregates were in saturated surface dry condition. Quartz ( $\text{SiO}_2$ ) was dominant phase in the fine aggregate, followed by calcite ( $\text{CaCO}_3$ ). Figures 1 and 2 show the XRD spectra and gradation curve of fine aggregate, respectively. The sand to binder ratio was 3, water to cement ratio was

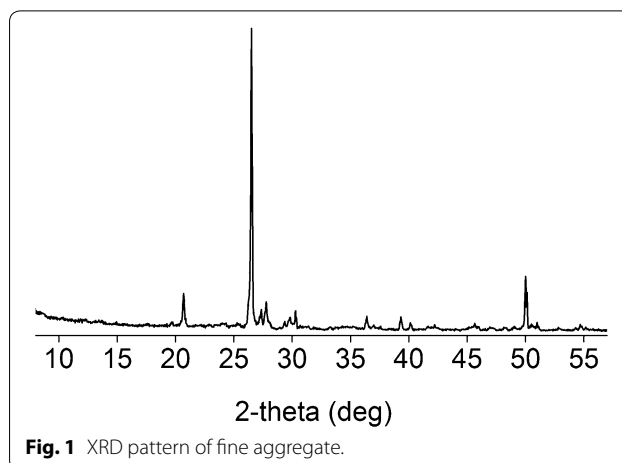


Fig. 1 XRD pattern of fine aggregate.

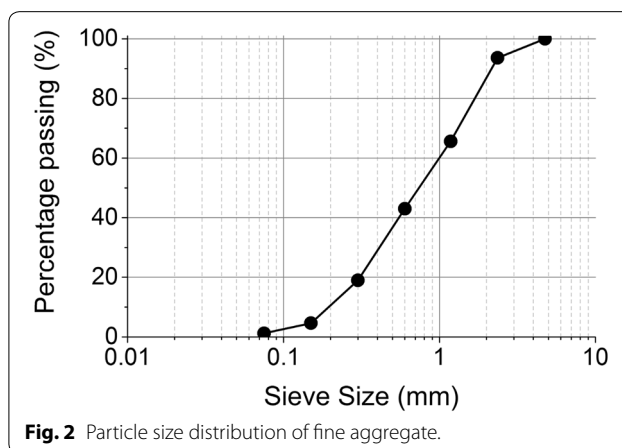


Fig. 2 Particle size distribution of fine aggregate.

0.45, and 3% of the weight of cement was replaced with  $\text{TiO}_2$ . Anatase and rutile are most used crystalline phases of  $\text{TiO}_2$  in cement based materials. Their effects on properties of cementitious materials are different (Staub de Melo and Trichês 2018). Anatase was chosen in this study because it shows more photocatalytic performance than rutile (Zhang et al. 2014). The amount of nano-silica varied between mortars; 0%, 0.5%, 1%, 1.5%, and 2% of weight of the cement. These mortars were denoted as S0, S1, S2, S3, and S4, respectively. The workability reduced with the addition of nano-silica, so additional superplasticizer was added to keep the flow of mortars within  $150 \pm 10$  mm. The dosage of superplasticizer was established after a number of trials with the help of flow table test, ASTM C1437 (ASTM 2007). The properties of  $\text{TiO}_2$  and nano-silica are given in Table 1. The nano- $\text{TiO}_2$  and nano-silica were dispersed in water separately. These nanoparticles were first dispersed in water using a magnetic stirrer for 3 h, then treated with horn ultrasonication (Sonic probe<sup>®</sup>, USA) for 45 min. The mix proportion is summarized in Table 2. Mortars were mixed in a laboratory mixer for 5 min, cast in cubes ( $5 \times 5 \times 5$  mm)

**Table 1 Properties of nano-titanium dioxide and nano-silica.**

Property	Nano-TiO <sub>2</sub>	Nano-SiO <sub>2</sub>
Particle size (nm)	10–60 nm	20–40 nm
Specific surface area (m <sup>2</sup> /g)	90	150
Weight (%)	Anatase ≥ 99.0	SiO <sub>2</sub> ≥ 99.0

**Table 2 Mix proportions.**

Mix proportion designation	TiO <sub>2</sub> (% of binder)	SiO <sub>2</sub> (% of binder)	w/b ratio	Superplasticizer (% of binder)
S0	3	0	0.45	0.4
S1	3	0.5	0.45	0.45
S2	3	1.0	0.45	0.5
S3	3	1.5	0.45	0.6
S4	3	2	0.45	0.7

and prisms (4 × 4 × 16 mm) and then compacted using a vibrating table. Mortars were demolded after 24 h. and put in saturated limewater for 90 days.

**2.2 Accelerated Leaching Test Setup**

The accelerated leaching test setup contained 6 M NH<sub>4</sub>NO<sub>3</sub> solution in glass tanks having corrugated test beds. The NH<sub>4</sub>NO<sub>3</sub> solution was continuously agitated and renewed after every 4th week. The test setup is shown in Fig. 3. For measuring the leaching depth, mortar cubes were equally divided into two parts at the center with a cutter machine as shown in Fig. 4. After spraying phenolphthalein solution on sliced mortar specimens, its central region turned into purple red indicating the sound part. The rest of gray peripheral area of the

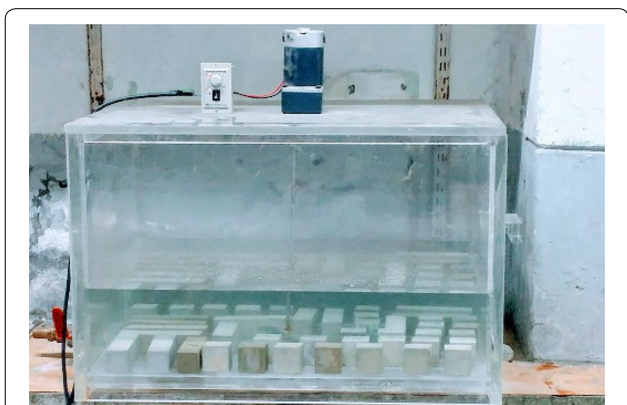


**Fig. 3** Mortar specimens immersed in 6 M NH<sub>4</sub>NO<sub>3</sub> solution in an acrylic tank.

specimens indicated leached area which was attacked by NH<sub>4</sub>NO<sub>3</sub>. The leaching depth was measured at each 5 mm interval on all sides of sliced mortar cubes and average value was reported. Leaching depth was calculated at different days of immersion (14, 28, 56, 84, 112, and 140 days).

Compressive strength, flexural strength and dynamic modulus of elasticity were evaluated according to ASTM C109, ASTM C348 and ASTM C597 (Testing and Cement 2013; ASTM 2002a, b). Mercury intrusion porosimetry was evaluated using Micromeritics Autopore IV 9500. Samples were dried using solvent exchange method (Ramachandran and Beaudoin 2000). Water porosity was measured using steps mentioned in (Fares et al. 2009). The Vickers microhardness test is used for the characterization of surface hardness (Igarashi et al. 1996; Qudoos et al. 2018). Microhardness values were measured after 56 and 140 days of leaching. Sliced cube samples (shown in Fig. 4) were used here for calculation of Vickers microhardness value. For this, first, sliced samples were polished with various grit polishing papers (400, 800, 1200, and 1500 successively) and then left to dry at room temperature for 24 h. A load of 0.1 kgf was applied on the polished surface using Vickers hardness tester, THV-1MD and maintained for 10 s. Microhardness values were measured at 5, 10, 15, 20, and 25 mm depths from the edge. A minimum of 10 readings were measured at each depth. The value of Vickers hardness is calculated according to Eq. (1):

$$HV = 1.854P/D^2 \tag{1}$$

where HV, P, D denote the Vickers hardness value (MPa), load (kgf), and the mean diagonal of the indentation pyramid (mm), respectively. For microstructural analyses, samples were obtained from the sliced cubes as shown in Fig. 4. Changes in the crystalline phases of mortars were identified with the help of X-ray diffraction. XRD pattern was acquired with a Rigaku diffractor upon powdered samples passed through 200-µm sieve. Thermogravimetric analysis is a popular technique for the measurement of CH in cement-based materials (Ramachandran 1979; Lam et al. 2000; Ramachandran and Beaudoin 2000). It

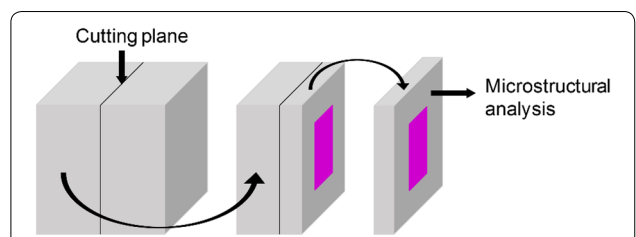
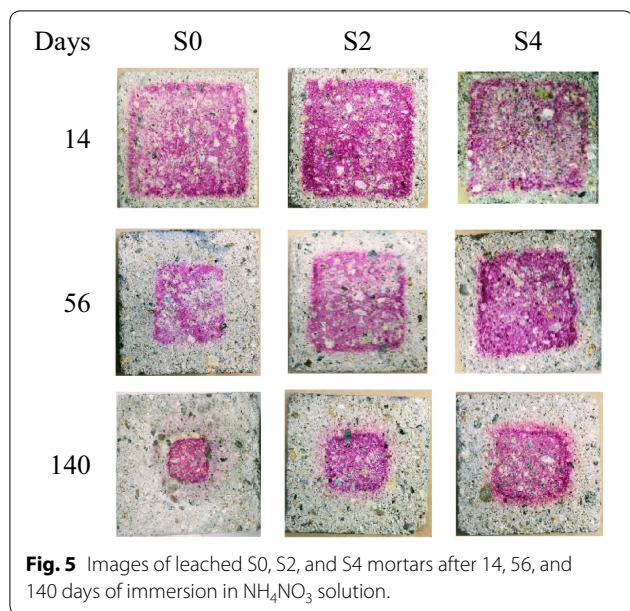


**Fig. 4** Determination of the leaching depth and obtaining of sample for microstructural analysis.



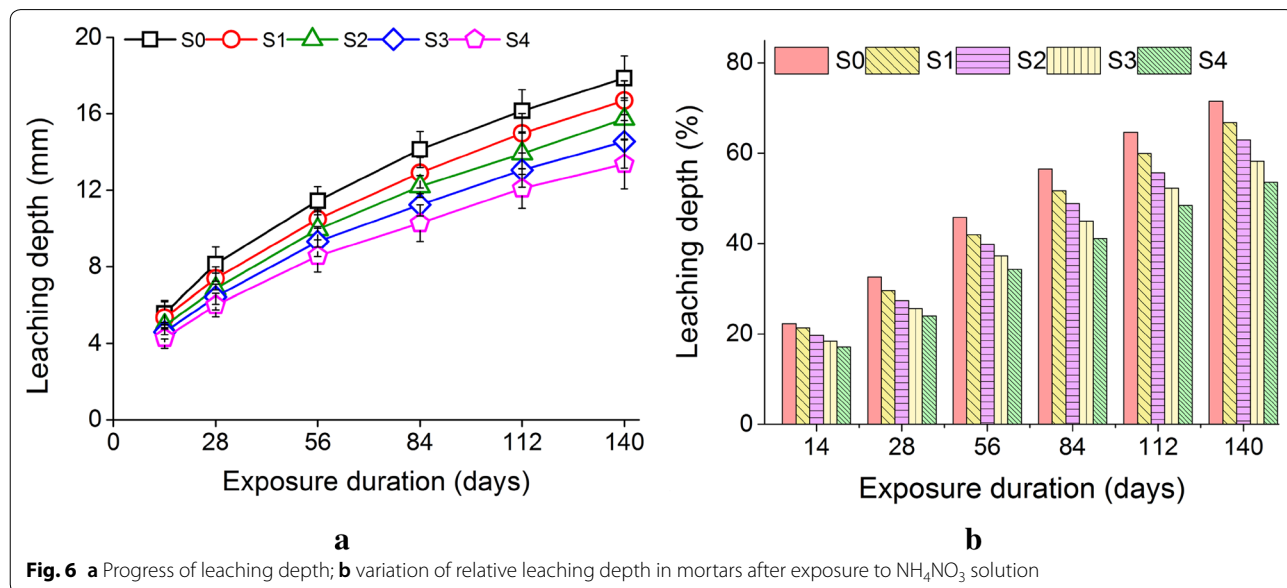
has been used for the measurement of CH content in the mortars at different intervals of leaching (Jain and Neithalath 2009). Powdered samples (10 mg) obtained from mortar specimens were heated at a rate of 10 °C/min, from room temperature to 800 °C in nitrogen atmosphere, using SDT Q600 Thermogravimetric Analyzer. Three samples were tested for each mix proportion type. The mass loss between 370 and 500 °C was expressed as percentage of sample weight at 600 °C and then normalized (Roychand et al. 2016). Changes in CSH gel were evaluated with the help of a Fourier transform infrared spectra using Thermo Scientific/IS50. Potassium bromide

(KBr) pellets of 12 mm dia were prepared and analyzed in the range of 400 to 4000  $\text{cm}^{-1}$  with a resolution of 4  $\text{cm}^{-1}$ . Morphology of the mortars was studied on the polished surface of mortars using Hitachi, S-3000 N, Scanning Electron Microscopy. SEM samples were prepared according to method discussed in (Brown and Sanchez 2016).

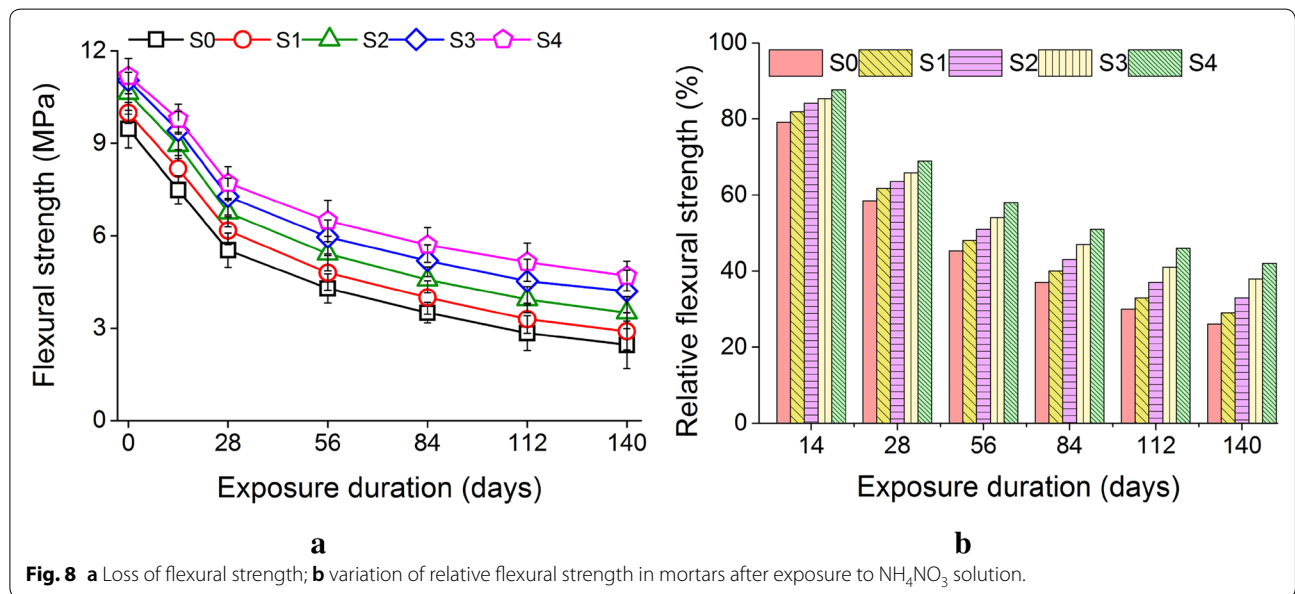
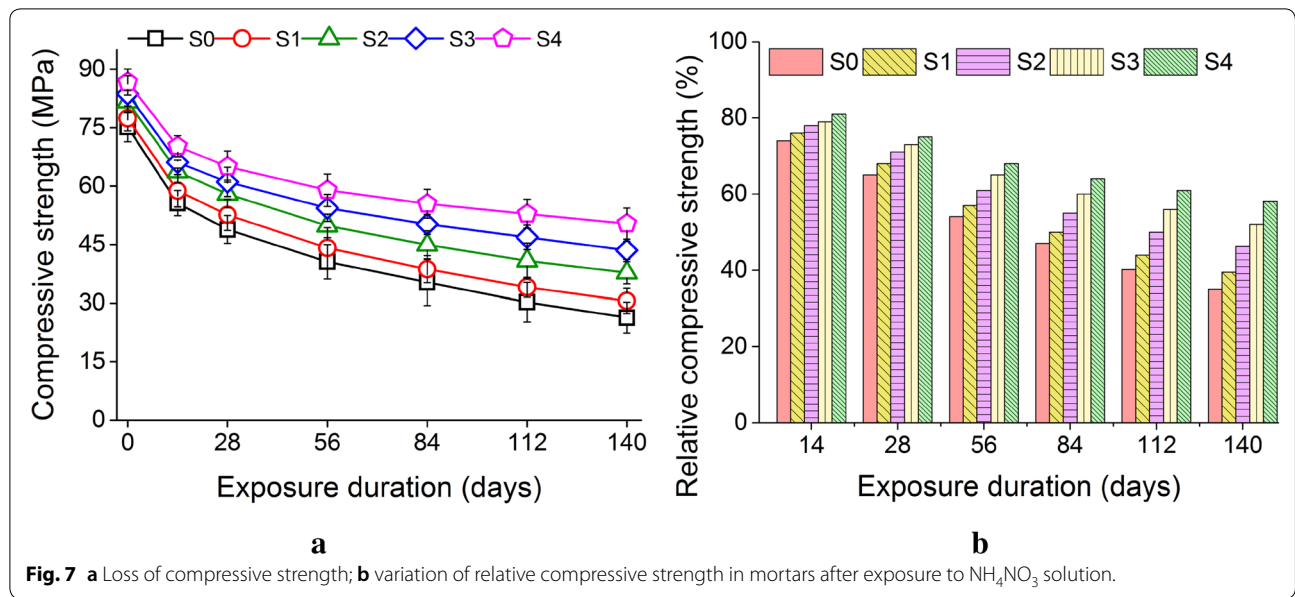
### 3 Results and Discussion

Figure 5 demonstrates the leaching depth in S0, S2, and S4 sliced mortars which were sprayed with phenolphthalein solution. These mortars have been immersed in  $\text{NH}_4\text{NO}_3$  solution for 14, 56, and 140 days. Two colors (grey and purple red) can be distinguished on the surface of mortars. Grey color shows decalcified zone while purple red shows safe core (Perlot et al. 2013; Segura et al. 2013; Xie et al. 2008). Progress of leaching depth is shown in Fig. 5a after 14, 28, 56, 84, 112, and 140 days of exposure to  $\text{NH}_4\text{NO}_3$  solution. Their relative leaching depths (with respect to initial uncalcified depth) are shown in Fig. 5b. An increase in leaching depth with exposure to aggressive environment is visible. Figure 6 clearly shows that the addition of nano-silica decreased the leaching depth in photocatalytic mortars.

The addition of nano-silica increased the mechanical properties of mortars as shown in Figs. 7 and 8. The loss of mechanical properties due to the leaching was evaluated by measuring the variations in compressive and flexural strength. Loss of compressive and flexural strengths are shown in Figs. 7a and 8a. It is apparent from the results that leaching attack deteriorated the mechanical properties of mortars. For the better interpretation of the results, relative compressive and flexural strengths of each mortar are shown in Figs. 7b and 8b. These



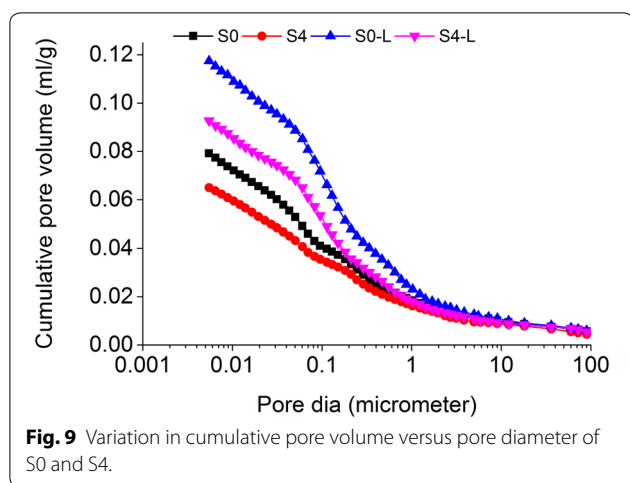




have been measured with respect to their compressive and flexural strengths before exposure to the leaching attack. Figure 8 indicate that the presence of nano-silica increased residual flexural strength in leached mortars.

Figure 9 shows the MIP results of S0 and S4 mortars (stored in saturated limewater), S0-L and S4-L (stored in  $\text{NH}_4\text{NO}_3$  solution for 140 days). Effects of adding nano-silica on the pore size distribution of cementitious materials is visible, nano-silica reduced the volume of pores in S4 mortar compared to S0. Previous researchers have also reported a reduction in the porosity and permeability of

mortars with the addition of nano-materials (Stefanidou and Papayianni 2012; Tobón et al. 2012; Jung et al. 2019). Nano-silica reacts with portlandite and reduces its quantity. The products of this pozzolanic reaction are secondary calcium-silicate-hydrate gels, formed in the pores of mortars and reduce the porosity (Nazari and Riahi 2011). Secondly, nano-silica acts as a filler and plugs the voids (Said et al. 2012). Leaching attack increased the volume of pores in S0 and S4 mortars. This effect was more visible in pores smaller than 10  $\mu\text{m}$ . The increase in pore volume between 0.003 and 0.01  $\mu\text{m}$  is attributed to



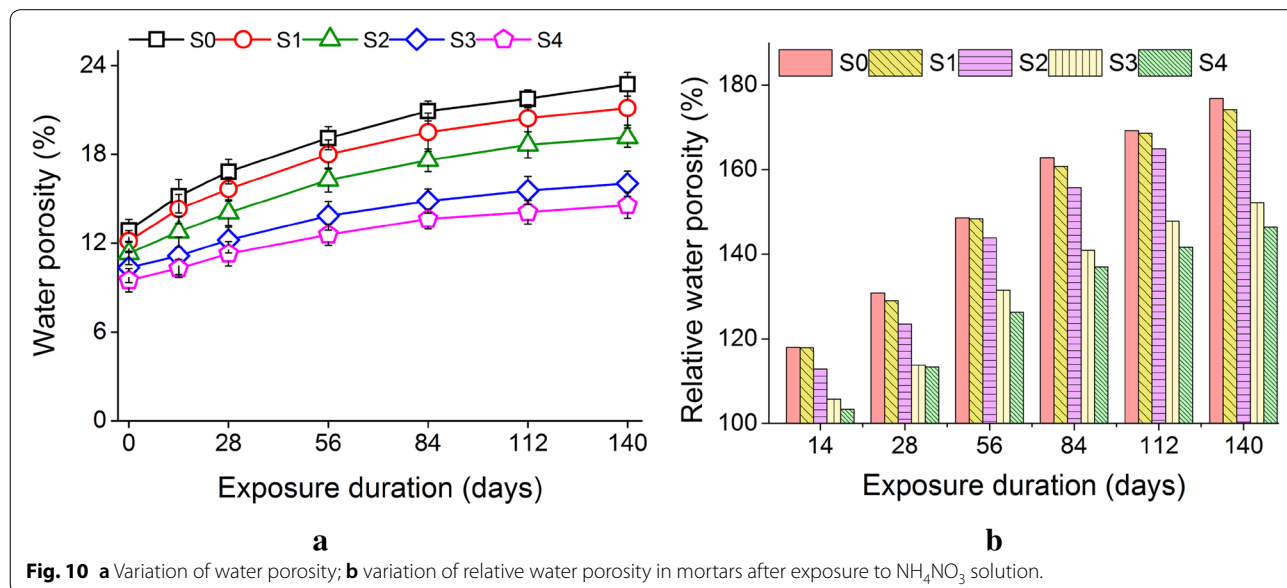
decalcification of calcium-silicate-hydrate gel. While the increase in number of pores between 0.01 and 100 μm is associated to dissolution of portlandite (Perlot et al. 2013; Phung et al. 2016). The cumulative pore volume of S4-L was lower than cumulative pore volume of S0-L due to less decalcification of CH and CSH in S4-L.

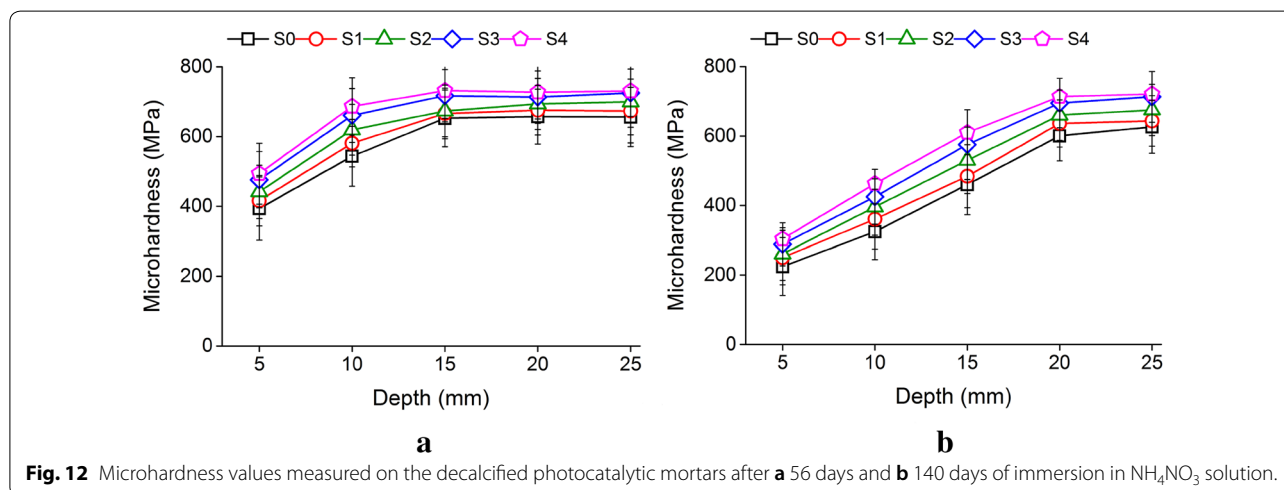
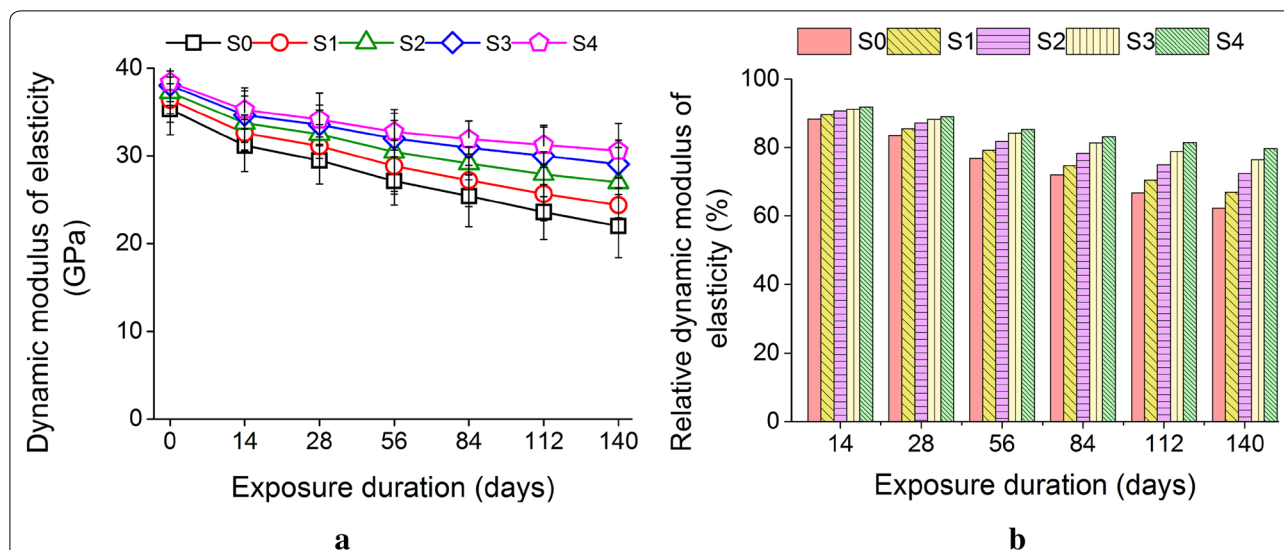
Figure 10a shows the changes in water porosity of mortars. This figure shows that the addition of nano-silica reduced the water porosity of mortars. This reduction in porosity is due to the filler and pozzolanic activity of nano-silica (Singh et al. 2017; Li et al. 2017; Singh et al. 2016). Figure 10a, b show that water porosity increased after immersion of mortars in NH<sub>4</sub>NO<sub>3</sub> solution. This is due to the decalcification of CH and CSH which produced more voids; increased the diameter of

existing voids and their connectivity (Phung et al. 2016). Macropores were produced due to the leaching of CH and micropores were produced due to decalcification of CSH (Escadeillas 2013).

Figure 11 shows the changes in dynamic modulus of elasticity of the mortars after exposure to NH<sub>4</sub>NO<sub>3</sub> solution. Dynamic modulus of elasticity test results can indicate the development of pores in the cement mortars due to the leaching attack (Lafhaj and Goueygou 2009). Figure 11 shows a linear increase in dynamic modulus of elasticity with the addition of nano-silica. Nano-silica is a filler material, so it filled the pores and decreased the porosity (Singh et al. 2016). Secondly, it is a pozzolanic material, it densified the microstructure and further reduced the porosity (Singh et al. 2017). The dynamic modulus of elasticity reduced after leaching attack. Figure 11b also shows that the relative dynamic modulus of elasticity decreased after the immersion of mortars in NH<sub>4</sub>NO<sub>3</sub>, but the addition of nano-silica reduced the loss of the dynamic modulus of elasticity in mortars.

Figure 12 shows the microhardness values measured on the polished surface of decalcified mortars after 56 and 140 days of immersion in NH<sub>4</sub>NO<sub>3</sub> solution. As the leaching starts from the peripheral areas and progresses towards the central zone, therefore peripheral leached area became weaker and showed lower values of microhardness than core part of the mortars. Microhardness results show that after 56 days of immersion, effected depth exceeded 10 mm, and after 140 days of immersion, effected depth exceeded 15 mm. Figure 12 suggests that resistance to the softening of the peripheral area due to leaching increased with the addition of nano-silica

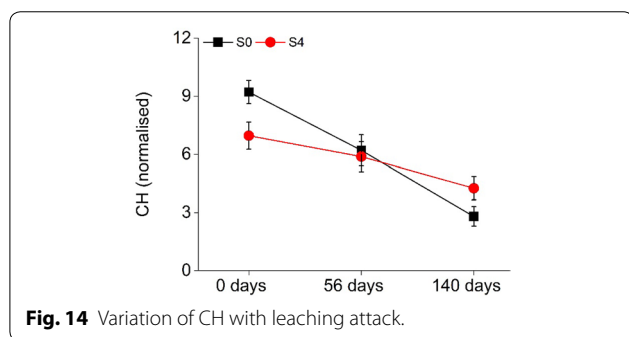
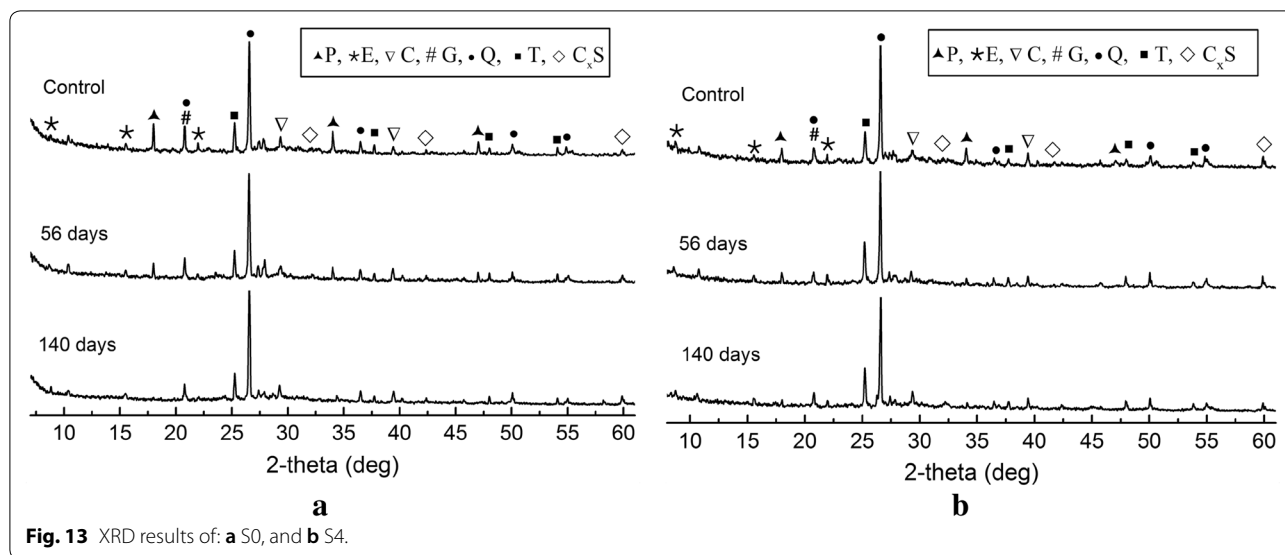




and it is consistent to the results of other macroscopic properties.

XRD results of S0 and S4 photocatalytic mortars immersed in saturated limewater and  $\text{NH}_4\text{NO}_3$  solution (for 56 and 140 days) are presented in Fig. 13. Saturated limewater represents controlled environment while  $\text{NH}_4\text{NO}_3$  solution represents leaching environment. Peaks of ettringite (E), gypsum (G), portlandite (P), calcium carbonate (C), unhydrated cement phases ( $\text{C}_x\text{S}$ ), quartz (Q), titanium dioxide (T) are illustrated in the XRD results. The peaks of portlandite reduced with leaching due to its dissolution in  $\text{NH}_4\text{NO}_3$  solution. Ettringite peaks were not affected, probably it was not dissolved (Carde et al. 1996; Tang et al. 2016; Han

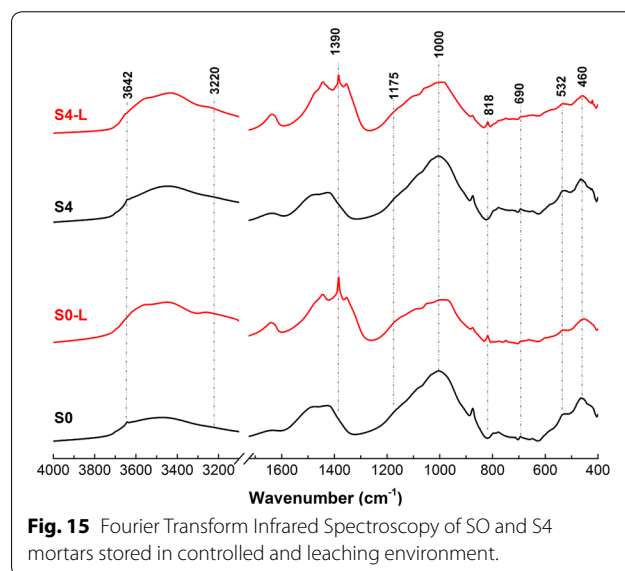
et al. 2014). Comparison of XRD patterns of S0 and S4 after 56 and 140 days of leaching shows that crystalline hydrated products were more deteriorated in S0 than S4. Portlandite peaks of S0 mortar eliminated after 140 days of decalcification. Nano-silica consumes portlandite during pozzolanic activity and also acts a filler of voids (Stefanidou and Papayianni 2012; Tobón et al. 2012; Nazari and Riahi 2011; Said et al. 2012). Both these properties made S4 mortar impermeable and consequently, retarded the penetration of hostile ions in it (Mohseni et al. 2016). As dissolution of portlandite, ettringite, calcium-silicate-hydrate gels occurs after reaction with penetrated ions (Escadeillas 2013; Kamali et al. 2008), but S4 was more impermeable to



these ions and had lesser portlandite. Hence, S4 mortar types were more stable than S0 mortars after exposure to  $\text{NH}_4\text{NO}_3$  solution.

S0 and S4 mortar specimens stored in controlled environment (saturated limewater) were studied using thermogravimetric analysis (TGA). Their exposure to leaching solution was null (0-day). For comparison, S0 and S4 mortar specimens stored for 56 and 140 days in  $\text{NH}_4\text{NO}_3$  solution were selected for TGA analysis. The content of portlandite in mortars is shown in Fig. 14. The reduction in portlandite content is visible after 56 and 140 days of decalcification. Previous studies observed a reduction in amount of portlandite through thermogravimetric analysis and attributed this to its dissolution (Marinoni et al. 2008). The reduction of portlandite varies among mortars. S0 shows a faster reduction of portlandite while S4 shows a slower reduction of portlandite.

FTIR spectra of S0 and S4 mortar samples are shown in Fig. 15, where S0 and S4 represent the mortars which were stored in controlled environment (saturated limewater), while S0-L and S4-L represent the mortars which



were stored in  $\text{NH}_4\text{NO}_3$  solution for 140 days. Study of the FTIR spectra indicates the variations in the chemistry of the mortars due to decalcification. Some new bands were evolved in FTIR spectra, frequency and intensity of the remaining bands varied due to the decalcification of portlandite and calcium-silicate-hydrate gel, polymerization of silicate and substitution of Si with Al in calcium-silicate-hydrate gel (Puertas et al. 2012). In FTIR spectra, each peak shows a specific vibration of a hydrated product. The band at  $3642\text{ cm}^{-1}$  is a result of the vibration of portlandite which disappeared in leached mortars due to leaching (Fernández Carrasco et al. 2012; Yu et al. 1999). In the S0-C and S4-C mortars, the band at  $1000\text{ cm}^{-1}$  is



the result of Si–O symmetric stretching vibration. After decalcification, this band shifted to 985 and 990  $\text{cm}^{-1}$  in S0-L and S4-L, respectively and its intensity was reduced. This shift of peak to lower frequencies is the result of the depolymerization of aluminosilicate or silicate networks in leached specimens (Yu et al. 1999; Lee and van Deventer 2002). The shifting of peak in S4-L is lesser than S0-L. This shows that S4-L was more stable than S0-L and it confirms the macroscopic tests that nano-silica containing photocatalytic mortars are more resistant to decalcification attack. A new band at 1390  $\text{cm}^{-1}$  has evolved due to the asymmetric stretching vibration of the  $\text{NO}_3^-$  group in  $\text{Ca}(\text{NO}_3)_2$  (Puertas et al. 2012). This band has a higher intensity in S0-L compared to S4-L. As  $\text{Ca}(\text{NO}_3)_2$  is a product of leaching attack (Escadeillas 2013), its higher peak in S0-L suggests that it was produced in more quantity in S0-L than S4-L. It verifies the better resistance of nano-silica containing photocatalytic mortars to leaching attack. The new bands at 818  $\text{cm}^{-1}$  and 1360  $\text{cm}^{-1}$  in the decalcified mortars are due to the stretching vibration of O–Al–O groups where Al had substituted Si at tetrahedral sites of calcium-silicate-hydrate gel (Hidalgo et al. 2007; López et al. 2008). Furthermore, in leached mortars, the shoulder at 1175  $\text{cm}^{-1}$  is due to the replacement of Si with Al in some calcium-silicate-hydrate gel and the formation of calcium aluminosilicate in mortars (Hidalgo et al. 2007; Andersen et al. 2004). The intensity of shoulders at 1055  $\text{cm}^{-1}$  increased due to the structural reorganization and depolymerization of calcium-silicate-hydrate gel (Lee and van Deventer 2002).  $\text{TiO}_2$  shows peaks around 420, 1620, and 3460  $\text{cm}^{-1}$  (Linstrom and Mallard 2001). However, in this study, separate peaks of  $\text{TiO}_2$  could not be distinguished because they have been overlapped with peaks of cement hydration products.

Figures 16 and 17 illustrate SEM images of S0 and S4 mortars stored in limewater and  $\text{NH}_4\text{NO}_3$  solution.

Comparison of Figs. 16a and 17a show that S4 has denser microstructure than S0. As stated earlier, it is due to the pozzolanic and filler effects of nano-silica (Stefanidou and Papayianni 2012; Tobón et al. 2012). SEM images show that exposure to  $\text{NH}_4\text{NO}_3$  solution created pores in the mortars and connected them. These pores were created due to dissolution of portlandite and calcium-silicate-hydrate (Phung et al. 2016; Escadeillas 2013). Previous researchers have also observed porous microstructure after leaching attack (Tang et al. 2016). Evaluation of Figs. 16b and 17b shows that S0 mortar became more porous than S4 after exposure to  $\text{NH}_4\text{NO}_3$  solution. This confirms nano-silica effectively increased the photocatalytic mortars' resistance to leaching. This is in consistent to the evaluation of hardened properties at various stages of leaching which showed that mortars became more resistant to decalcification with the addition of nano-silica.

Incorporation of nano-silica improved the resistance of photocatalytic mortars to the decalcification attack. As the amount of nano-silica increased in the mortars, the loss of mechanical and physical properties due to the leaching attack reduced. Similarly, the microstructure of the mortars containing nano-silica was more stable after leaching attack. The increase in leaching resistance is due to the synergetic effects which were created in the mortars due to addition of nano-silica. First, nano-silica particles are of very small size, these particles perform as nuclei for cement hydration reaction. Cement hydration products are formed around these particles and pores are occupied. This leads to the refinement of pore structure (Singh et al. 2013; Chen et al. 2012). Second, nano-silica can act as a filler and fill the voids (Sanchez and Sobolev 2010). As decalcification process involves the dissolution of hydration products and then their diffusion to the outside aggressive environment (Phung et al. 2016). The

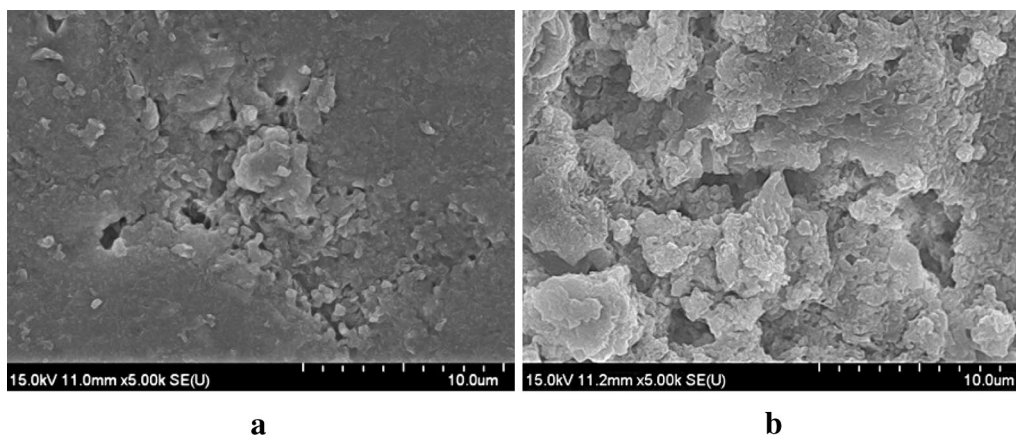


**Fig. 16** Morphology of S0 mortar stored in **a** limewater and **b**  $\text{NH}_4\text{NO}_3$  solution for 140 days.

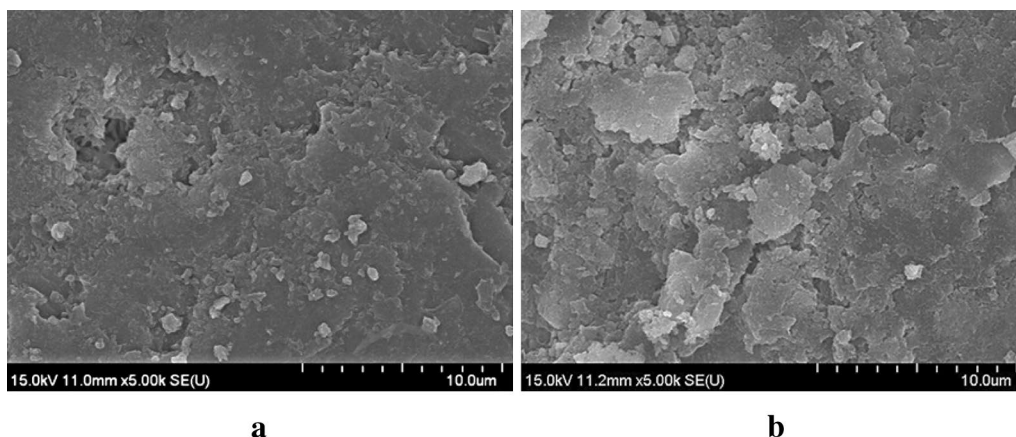


**Fig. 17** Morphology of S4 mortar stored in **a** limewater and **b**  $\text{NH}_4\text{NO}_3$  solution for 140 days.

presence of nano-silica reduces the pores and decreases the permeability, therefore the penetration of aggressive ions and diffusion of  $\text{Ca}^{2+}$  ions is hindered. Third, nano-silica acts as a pozzolanic material. It consumes portlandite and produces calcium-silicate-hydrate gel (Singh et al. 2013). Numerous previous studies have reported that portlandite is the most vulnerable hydration product during leaching attack (Escadeillas 2013). With the addition of nano-silica, the amount of vulnerable portlandite is reduced due to pozzolanic effect of nano-silica and leaching was further reduced.

#### 4 Conclusion

This study focused on the decalcification attack upon photocatalytic cement mortars after incorporating 0%, 0.5%, 1.0%, 1.5%, and 2.0% nano-silica. A concentrated solution of ammonium nitrate ( $\text{NH}_4\text{NO}_3$ ) was used as aggressive medium. The evolution of leaching depth, the variation of compressive and flexural strengths, porosity, dynamic modulus of elasticity and microhardness values were measured. Microstructural analysis like FTIR, SEM, EDS, XRD, TGA tests were conducted on unleached and leached specimens.

1. Leaching depth decreased with the addition of nano-silica in photocatalytic mortars. Reduction of compressive and flexural strengths and increase in porosity were observed but these leaching effects were reduced with the increase in amount of nano-silica in mortars. Addition of nano-silica decreased the changes in dynamic modulus of elasticity and microhardness due to leaching. Nano-silica resists the degradation of hardened properties of cementitious materials in a leaching environment.

2. XRD and TGA results showed leaching of portlandite, FTIR results presented the decalcification of calcium-silicate-hydrate gel, SEM observations confirmed the increase in amount of micropores. But these microstructural changes were reduced as the amount of nano-silica increased in mortars. Addition of nano-silica resists microstructural changes during leaching attack.
3. Nano-silica can be added in photocatalytic cementitious materials to resist deterioration due to leaching attack.
4. Future studies can focus on potential effects of adding nano-silica on the performance of cementitious materials and geopolymers in simulated acid rain solutions and sulfate solutions.

#### Authors' contributions

AR, AQ, SHJ conceived, designed and performed this experimental study under the guidance and supervision of JSR. HGK helped in writing the manuscript. All authors read and approved the final manuscript.

#### Availability of data and materials

The datasets used and/or analyzed during the current study are available from the corresponding author on reasonable request.

#### Competing interests

The authors declare that they have no competing interests.

Received: 22 February 2019 Accepted: 13 May 2019

Published online: 03 June 2019

#### References

- Andersen, M. D., Jakobsen, H. J., & Skibsted, J. (2004). Characterization of white Portland cement hydration and the C-S-H structure in the presence of sodium aluminate by  $^{27}\text{Al}$  and  $^{29}\text{Si}$  MAS NMR spectroscopy. *Cement and Concrete Research*, 34, 857–868.

- Astm, C. (2002a). 348-02: Standard test method for flexural strength and modulus of hydraulic cement mortars. West Conshohocken: ASTM.
- Astm, C. (2002b). 597. Standard test method for pulse velocity through concrete. West Conshohocken: ASTM International.
- Astm, C. J. C. (2007). Standard test method for flow of hydraulic cement mortar.
- Atta-Ur-Rehman, Qudoos, A., Kim, H. G., & Ryou, J.-S. (2018). Influence of titanium dioxide nanoparticles on the sulfate attack upon ordinary portland cement and slag-blended mortars. *Materials*, 11, 356.
- Banerjee, S., Dionysiou, D. D., & Pillai, S. C. (2015). Self-cleaning applications of TiO<sub>2</sub> by photo-induced hydrophilicity and photocatalysis. *Applied Catalysis, B: Environmental*, 176–177, 396–428.
- Berger, S., Aouad, G., Cau Dit Coumes, C., Le Bescop, P., & Damidot, D. (2013). Leaching of calcium sulfoaluminate cement pastes by water at regulated pH and temperature: Experimental investigation and modeling. *Cement and Concrete Research*, 53, 211–220.
- Binas, V., Papadaki, D., Maggos, T., Katsanaki, A., & Kiriakidis, G. (2018). Study of innovative photocatalytic cement based coatings: The effect of supporting materials. *Construction and Building Materials*, 168, 923–930.
- Brown, L., & Sanchez, F. (2016). Influence of carbon nanofiber clustering on the chemo-mechanical behavior of cement pastes. *Cement & Concrete Composites*, 65, 101–109.
- Carde, C., François, R., & Torrenti, J.-M. (1996). Leaching of both calcium hydroxide and C-S-H from cement paste: Modeling the mechanical behavior. *Cement and Concrete Research*, 26, 1257–1268.
- Chen, J., Kou, S.-C., & Poon, C.-S. (2012). Hydration and properties of nano-TiO<sub>2</sub> blended cement composites. *Cement & Concrete Composites*, 34, 642–649.
- Diamanti, M. V., Paolini, R., Rossini, M., Aslan, A. B., Zinzi, M., Poli, T., et al. (2015). Long term self-cleaning and photocatalytic performance of anatase added mortars exposed to the urban environment. *Construction and Building Materials*, 96, 270–278.
- Eom, T. S., Park, E. J., & Lee, S. J. (2019). Shear behavior of reinforced concrete structural walls subjected to eccentric axial compression. *Journal of the Korea Concrete Institute*, 31, 11–20.
- Escadellias, G. (2013). Ammonium nitrate attack on cementitious materials. In *Performance of cement-based materials in aggressive aqueous environments*. Berlin: Springer.
- Fares, H., Noumowe, A., & Remond, S. (2009). Self-consolidating concrete subjected to high temperature: Mechanical and physicochemical properties. *Cement and Concrete Research*, 39, 1230–1238.
- Fernández Carrasco, L., Torrens Martín, D., Morales, L., & Martínez Ramírez, S. (2012). *Infrared spectroscopy in the analysis of building and construction materials*. Londong: InTech.
- García, L. D., Pastor, J. M., & Peña, J. (2018). Self cleaning and depolluting glass reinforced concrete panels: Fabrication, optimization and durability evaluation. *Construction and Building Materials*, 162, 9–19.
- Guo, M.-Z., & Poon, C. S. (2018). Superior photocatalytic NO<sub>x</sub> removal of cementitious materials prepared with white cement over ordinary Portland cement and the underlying mechanisms. *Cement & Concrete Composites*, 90, 42–49.
- Han, F., Liu, R., & Yan, P. (2014). Effect of fresh water leaching on the microstructure of hardened composite binder pastes. *Construction and Building Materials*, 68, 630–636.
- Han, B., Zhang, L., & Ou, J. (2017). *Smart and multifunctional concrete toward sustainable infrastructures*. Berlin: Springer.
- Hassan, M. M., Dylla, H., Mohammad, L. N., & Rupnow, T. (2010). Evaluation of the durability of titanium dioxide photocatalyst coating for concrete pavement. *Construction and Building Materials*, 24, 1456–1461.
- Hidalgo, A., Petit, S., Domingo, C., Alonso, C., & Andrade, C. (2007). Microstructural characterization of leaching effects in cement pastes due to neutralisation of their alkaline nature: Part I: Portland cement pastes. *Cement and Concrete Research*, 37, 63–70.
- Igarashi, S., Bentur, A., & Mindess, S. (1996). Microhardness testing of cementitious materials. *Advanced Cement Based Materials*, 4, 48–57.
- Jain, J., & Neithalath, N. (2009). Analysis of calcium leaching behavior of plain and modified cement pastes in pure water. *Cement & Concrete Composites*, 31, 176–185.
- Jung, M., Lee, Y. S., & Hong, S. G. (2019). Study on improvement in electromagnetic interference shielding effectiveness of ultra-high performance concrete (UHPC)/carbon nanotube (CNT) composites. *Journal of the Korea Concrete Institute*, 31, 69–77.
- Kamali, S., Moranville, M., & Leclercq, S. (2008). Material and environmental parameter effects on the leaching of cement pastes: Experiments and modelling. *Cement and Concrete Research*, 38, 575–585.
- Khaloo, A., Mobini, M. H., & Hosseini, P. (2016). Influence of different types of nano-SiO<sub>2</sub> particles on properties of high-performance concrete. *Construction and Building Materials*, 113, 188–201.
- Lafhaj, Z., & Goueygou, M. (2009). Experimental study on sound and damaged mortar: Variation of ultrasonic parameters with porosity. *Construction and Building Materials*, 23, 953–958.
- Lam, L., Wong, Y. L., & Poon, C. S. (2000). Degree of hydration and gel/space ratio of high-volume fly ash/cement systems. *Cement and Concrete Research*, 30, 747–756.
- Lee, W. K. W., & Van Deventer, J. S. J. (2002). Structural reorganisation of class F fly ash in alkaline silicate solutions. *Colloids and Surfaces A: Physicochemical and Engineering Aspects*, 211, 49–66.
- Li, Z., Ding, S., Yu, X., Han, B., & Ou, J. (2018). Multifunctional cementitious composites modified with nano titanium dioxide: A review. *Composites Part A: Applied Science and Manufacturing*, 111, 115–137.
- Li, L. G., Huang, Z. H., Zhu, J., Kwan, A. K. H., & Chen, H. Y. (2017). Synergistic effects of micro-silica and nano-silica on strength and microstructure of mortar. *Construction and Building Materials*, 140, 229–238.
- Linstrom, P. J. & Mallard, W. (2001). NIST Chemistry webbook; NIST standard reference database No. 69.
- López, A. H., Calvo, J. L. G., Olmo, J. G., Petit, S., & Alonso, M. C. (2008). Microstructural evolution of calcium aluminate cements hydration with silica fume and fly ash additions by scanning electron microscopy, and mid and near-infrared spectroscopy. *Journal of the American Ceramic Society*, 91, 1258–1265.
- Marinoni, N., Pavese, A., Voltolini, M., & Merlini, M. (2008). Long-term leaching test in concretes: An X-ray powder diffraction study. *Cement & Concrete Composites*, 30, 700–705.
- Mendoza, C., Valle, A., Castellote, M., Bahamonde, A., & Faraldos, M. (2015). TiO<sub>2</sub> and TiO<sub>2</sub>-SiO<sub>2</sub> coated cement: Comparison of mechanic and photocatalytic properties. *Applied Catalysis, B: Environmental*, 178, 155–164.
- Mohseni, E., Miyandehi, B. M., Yang, J., & Yazdi, M. A. (2015). Single and combined effects of nano-SiO<sub>2</sub>, nano-Al<sub>2</sub>O<sub>3</sub> and nano-TiO<sub>2</sub> on the mechanical, rheological and durability properties of self-compacting mortar containing fly ash. *Construction and Building Materials*, 84, 331–340.
- Mohseni, E., Naseri, F., Amjadi, R., Khotbehsara, M. M., & Ranjbar, M. M. (2016). Microstructure and durability properties of cement mortars containing nano-TiO<sub>2</sub> and rice husk ash. *Construction and Building Materials*, 114, 656–664.
- Nazari, A., & Riahi, S. (2011). The effects of SiO<sub>2</sub> nanoparticles on physical and mechanical properties of high strength compacting concrete. *Composites Part B: Engineering*, 42, 570–578.
- Paolini, R., Borroni, D., Pedferri, M., & Diamanti, M. V. (2018). Self-cleaning building materials: The multifaceted effects of titanium dioxide. *Construction and Building Materials*, 182, 126–133.
- Park, M. J., Lee, B. J., Kim, J. S., & Kim, Y. Y. (2018). Effect of concrete strength on chloride ion penetration resistance and chemical resistance of concrete coated by siloxane-based water repellent. *Journal of the Korea Concrete Institute*, 30, 583–590.
- Perlot, C., Carcassès, M., & Verdier, J. (2013). Diffusivity evolution under decalcification: Influence of aggregate natures and cement type. *Materials and Structures*, 46, 787–801.
- Phung, Q. T., Maes, N., Jacques, D., De Schutter, G., & Ye, G. (2016). Investigation of the changes in microstructure and transport properties of leached cement pastes accounting for mix composition. *Cement and Concrete Research*, 79, 217–234.
- Pozo-Antonio, J. S., & Dionísio, A. (2017). Self-cleaning property of mortars with TiO<sub>2</sub> addition using real diesel exhaust soot. *Journal of Cleaner Production*, 161, 850–859.
- Puertas, F., Goñi, S., Hernández, M. S., Varga, C., & Guerrero, A. (2012). Comparative study of accelerated decalcification process among C3S, grey and white cement pastes. *Cement & Concrete Composites*, 34, 384–391.
- Qudoos, A., Atta Ur, R., Kim, H. G., & Ryou, J.-S. (2018). Influence of the surface roughness of crushed natural aggregates on the microhardness of the interfacial transition zone of concrete with mineral admixtures and polymer latex. *Construction and Building Materials*, 168, 946–957.

- Ramachandran, V. S. (1979). Differential thermal method of estimating calcium hydroxide in calcium silicate and cement pastes. *Cement and Concrete Research*, 9, 677–684.
- Ramachandran, V. S., & Beaudoin, J. J. (2000). *Handbook of analytical techniques in concrete science and technology: Principles, techniques and applications*. Amsterdam: Elsevier.
- Roychand, R., De Silva, S., Law, D., & Setunge, S. (2016). High volume fly ash cement composite modified with nano silica, hydrated lime and set accelerator. *Materials and Structures*, 49, 1997–2008.
- Said, A. M., Zeidan, M. S., Bassuoni, M. T., & Tian, Y. (2012). Properties of concrete incorporating nano-silica. *Construction and Building Materials*, 36, 838–844.
- Sanchez, F., & Sobolev, K. (2010). Nanotechnology in concrete—A review. *Construction and Building Materials*, 24, 2060–2071.
- Segura, I., Molero, M., Aparicio, S., Anaya, J. J., & Moragues, A. (2013). Decalcification of cement mortars: Characterisation and modelling. *Cement & Concrete Composites*, 35, 136–150.
- Senff, L., Hotza, D., Lucas, S., Ferreira, V. M., & Labrincha, J. A. (2012). Effect of nano-SiO<sub>2</sub> and nano-TiO<sub>2</sub> addition on the rheological behavior and the hardened properties of cement mortars. *Materials Science and Engineering A*, 532, 354–361.
- Seo, D., & Yun, T. S. (2017). NO<sub>x</sub> removal rate of photocatalytic cementitious materials with TiO<sub>2</sub> in wet condition. *Building and Environment*, 112, 233–240.
- Sikora, P., Cendrowski, K., Markowska-Szczupak, A., Horszczaruk, E., & Mijowska, E. (2017). The effects of silica/titania nanocomposite on the mechanical and bactericidal properties of cement mortars. *Construction and Building Materials*, 150, 738–746.
- Singh, L. P., Ali, D., & Sharma, U. (2016). Studies on optimization of silica nanoparticles dosage in cementitious system. *Cement & Concrete Composites*, 70, 60–68.
- Singh, L. P., Karade, S. R., Bhattacharyya, S. K., Yousuf, M. M., & Ahalawat, S. (2013). Beneficial role of nanosilica in cement based materials—A review. *Construction and Building Materials*, 47, 1069–1077.
- Singh, L. P., Zhu, W., Howind, T., & Sharma, U. (2017). Quantification and characterization of C-S-H in silica nanoparticles incorporated cementitious system. *Cement & Concrete Composites*, 79, 106–116.
- Staub de Melo, J. V., & Trichês, G. (2018). Study of the influence of nano-TiO<sub>2</sub> on the properties of Portland cement concrete for application on road surfaces. *Road Materials and Pavement Design*, 19, 1011–1026.
- Stefanidou, M., & Papayianni, I. (2012). Influence of nano-SiO<sub>2</sub> on the Portland cement pastes. *Composites Part B: Engineering*, 43, 2706–2710.
- Tang, Y.-J., Zuo, X.-B., He, S.-L., Ayinde, O., & Yin, G.-J. (2016). Influence of slag content and water-binder ratio on leaching behavior of cement pastes. *Construction and Building Materials*, 129, 61–69.
- Testing, A. S. F., & Cement, M. C. C.-O. (2013). *Standard test method for compressive strength of hydraulic cement mortars (using 2-in/ or [50-mm] cube specimens)*. West Conshohocken: ASTM International.
- Tobaldi, D. M., Graziani, L., Seabra, M. P., Hennetier, L., Ferreira, P., Quagliarini, E., et al. (2017). Functionalised exposed building materials: Self-cleaning, photocatalytic and biofouling abilities. *Ceramics International*, 43, 10316–10325.
- Tobón, J. I., Payá, J. J., Borrachero, M. V., & Restrepo, O. J. (2012). Mineralogical evolution of Portland cement blended with silica nanoparticles and its effect on mechanical strength. *Construction and Building Materials*, 36, 736–742.
- Wang, D., Hou, P., Zhang, L., Xie, N., Yang, P., & Cheng, X. (2018). Photocatalytic activities and chemically-bonded mechanism of SiO<sub>2</sub>@TiO<sub>2</sub> nanocomposites coated cement-based materials. *Materials Research Bulletin*, 102, 262–268.
- Xie, S. Y., Shao, J. F., & Burlion, N. (2008). Experimental study of mechanical behaviour of cement paste under compressive stress and chemical degradation. *Cement and Concrete Research*, 38, 1416–1423.
- Xiong, C., Jiang, L., Xu, Y., Chu, H., Jin, M., & Zhang, Y. (2016). Deterioration of pastes exposed to leaching, external sulfate attack and the dual actions. *Construction and Building Materials*, 116, 52–62.
- Yang, H. J., Shim, H. B., Jin, S. H., & Ann, K. Y. (2018). Evaluation of rate of chloride transport for alumina cement mortar with different composition of clinkers. *Journal of the Korea Concrete Institute*, 30, 383–390.
- Yu, P., Kirkpatrick, R. J., Poe, B., Mcmillan, P. F., & Cong, X. (1999). Structure of calcium silicate hydrate (C-S-H): Near-, mid-, and far-infrared spectroscopy. *Journal of the American Ceramic Society*, 82, 742–748.
- Zhang, L., Ma, N., Wang, Y., Han, B., Cui, X., Yu, X., et al. (2016). Study on the reinforcing mechanisms of nano silica to cement-based materials with theoretical calculation and experimental evidence. *Journal of Composite Materials*, 50, 4135–4146.
- Zhang, J., Zhou, P., Liu, J., & Yu, J. (2014). New understanding of the difference of photocatalytic activity among anatase, rutile and brookite TiO<sub>2</sub>. *Physical Chemistry Chemical Physics*, 16, 20382–20386.

## Publisher's Note

Springer Nature remains neutral with regard to jurisdictional claims in published maps and institutional affiliations.

Submit your manuscript to a SpringerOpen<sup>®</sup> journal and benefit from:

- Convenient online submission
- Rigorous peer review
- Open access: articles freely available online
- High visibility within the field
- Retaining the copyright to your article

Submit your next manuscript at ► [springeropen.com](https://www.springeropen.com)